Письма в ЭЧАЯ. 2015. Т. 12, № 5(196). С. 1086–1099

ФИЗИКА ЭЛЕМЕНТАРНЫХ ЧАСТИЦ И АТОМНОГО ЯДРА. ЭКСПЕРИМЕНТ

INELASTIC SCATTERING AND MULTINUCLEON TRANSFER IN ^{3,4}He + ^{9}Be REACTIONS

A. S. Denikin [a, b, 1], *S. M. Lukyanov* [b], *N. K. Skobelev* [b], *Yu. G. Sobolev* [b], *E. I. Voskoboynik* [b], *Yu. E. Penionzhkevich* [b, c], *W. H. Trzaska* [d], *G. P. Tyurin* [d], *V. Burjan* [e], *V. Kroha* [e], *J. Mrázek* [e], *Š. Piskoř* [e], *V. Glagolev* [e], *Yi Xu* [e], *S. V. Khlebnikov* [f], *M. N. Harakeh* [g], *K. A. Kuterbekov* [h, i], *Yu. Tuleushev* [i]

[a] International University "Dubna", Dubna, Russia

[b] Joint Institute for Nuclear Research, Dubna

[c] National Research Nuclear University MEPhI, Moscow

[d] Department of Physics, University of Jyväskylä, Jyväskylä, Finland

[e] Nuclear Physics Institute, Řež, Czech Republic

[f] Khlopin Institute, St. Petersburg, Russia

[g] Kernfysisch Versneller Instituut, University of Groningen, Groningen, Netherlands

[h] Eurasian Gumilev University, Astana

[i] Nuclear Physics Institute, Almaty, Kazakhstan

A study of inelastic scattering and multinucleon transfer reactions was performed by α and ^{3}He beams on a ^{9}Be target at energy about 50 MeV. Angular distributions of the differential cross sections for the $^{9}\mathrm{Be}\,(\alpha,\alpha')\,^{9}\mathrm{Be}^{*}$, $^{9}\mathrm{Be}\,(\alpha,\,^{3}\mathrm{He})\,^{10}\mathrm{Be}$, $^{9}\mathrm{Be}\,(\alpha,t)\,^{10}\mathrm{B}$, $^{9}\mathrm{Be}\,(^{3}\mathrm{He},^{6}\mathrm{Li})\,^{6}\mathrm{Li}$, and $^{9}\mathrm{Be}\,(^{3}\mathrm{He},^{6}\mathrm{Be})\,^{6}\mathrm{He}$ reactions were measured. Experimental angular distributions of the differential cross sections for the ground state and a few low-lying states were analyzed in the framework of the optical model, coupled channels, and distorted-wave Born approximation. The information on the cluster structure of the reaction products was obtained. The analysis of the obtained spectroscopic factors was performed.

Изучено неупругое рассеяние и реакции многонуклонных передач при взаимодействии α-частиц и ^{3}He на ядрах мишени ^{9}Be при энергии 50 МэВ. Измерено угловое распределение дифференциальных сечений для реакций $^{9}\mathrm{Be}\,(\alpha,\alpha')\,^{9}\mathrm{Be}^{*}$, $^{9}\mathrm{Be}\,(\alpha,\,^{3}\mathrm{He})\,^{10}\mathrm{Be}$, $^{9}\mathrm{Be}\,(\alpha,t)\,^{10}\mathrm{B}$, $^{9}\mathrm{Be}\,(^{3}\mathrm{He},^{6}\mathrm{Li})\,^{6}\mathrm{Li}$ и $^{9}\mathrm{Be}\,(^{3}\mathrm{He},^{6}\mathrm{Be})\,^{6}\mathrm{He}$. Проанализированы экспериментальные угловые распределения дифференциальных сечений для основного и низколежащих возбужденных состояний в рамках оптической модели с использованием метода искаженных волн DWBA и метода учета спаренных каналов CC. Получена информация о кластерной структуре продуктов реакции. Произведен анализ полученных спектроскопических факторов.

PACS: 21.10.-k; 13.85.Fb; 25.45.Hi

[1] E-mail: denikin@jinr.ru

INTRODUCTION

In recent years, the study of light weakly bound nuclei [1–3] was intensified due to the significant progress made with radioactive beam facilities. It has been shown that in light nuclei the nucleons tend to group into clusters, whose relative motion mainly defines the properties of these nuclei. Along with unstable nuclei, the interest in the study of light stable nuclei has been renewed. The cluster structures of the ground, as well as low-lying excited states of these nuclei, are in the focus of studies. As examples, ^{6}Li and ^{7}Li nuclei are both well described by two-body cluster models ($\alpha+d$ and $\alpha+t$, respectively). Another interesting nuclide is ^{9}Be, which is usually treated as an $\alpha+n+\alpha$ three-body configuration; at the same time, one may also suppose different two-body configuration $^{8}\mathrm{Be}+n$ or $^{5}\mathrm{He}+\alpha$ for the excited states of ^{9}Be. The addition of a second valence neutron to ^{9}Be leads to another interesting nucleus, ^{10}Be, where the $^{6}\mathrm{He}+\alpha$ and the $^{5}\mathrm{He}+{}^{5}\mathrm{He}$ configurations together with the $\alpha+n+n+\alpha$ one may play an important role.

Recently, special attention has been focused on the role of the extra "valence" nucleons and their influence on the cluster structure of the excited states. This subject is discussed, for example, in [4], where the two-center molecular states in ^{9}B, ^{9}Be, ^{10}Be, and ^{10}B nuclei were considered in the framework of a molecular-type model.

The standard tool to study nuclear structure is the scattering of the projectiles, like the protons or ^{3,4}He, by a target nucleus, the structure of which is going to be studied. This method is based on the angular-distribution measurements of the projectile-like products with fixed excitation energy in the (in)elastic and transfer reaction channels.

This work is an attempt to shed light on the internal structure of ^{9,10}Be and ^{10}B nuclei, as well as on the mechanism of the nucleon–cluster transfers by the study of the ^{3,4}He induced reactions with the ^{9}Be target. We expected that the sensitivity of the high-precision scattering data to the cluster nuclear structure of light nuclei could be demonstrated. In this work, we supplement the data measured before [5–7] with the new ones extending the ranges of the exciting energy and scattering angle of the products. The performed data analysis is based on the optical model (OM), distorted-wave Born approximation (DWBA), and coupled-channel (CC) approach.

1. EXPERIMENTAL PROCEDURE

1.1. α (63 MeV) + ^{9}Be Measurements. First run of the $\alpha+{}^{9}$Be experiments was performed at the K130 Cyclotron facility of the Accelerator Laboratory of the Physics Department of Jyväskylä University and in the Nuclear Physics Institute (NPI), Řež, Czech Republic. The beam energy of ^{4}He ions was 63 MeV. The average beam current during the experiment was maintained at 3 nA. The self-supporting Be target was prepared from a 99% pure thin foil of beryllium. The target thickness was 12 μm. Peaks due to carbon and oxygen contaminations were not observed in the energy spectra.

To measure (in)elastically scattered ions, two telescopes each consisting of Si–Si(Li) detectors with thicknesses of 100 μm and 3 mm, respectively, were used. Each pair of detectors was mounted at a distance of about 45 cm from the target. Particle identification was performed based on the energy-loss measurements of ΔE and residual energy E_r, i.e., the so-called $\Delta E-E$ method. The Si-telescopes were mounted on rotating supports, which allowed one to obtain data from $\theta_{\mathrm{lab}}=20^{\circ}$ to $\theta_{\mathrm{lab}}=107^{\circ}$ in steps of $1-2^{\circ}$.

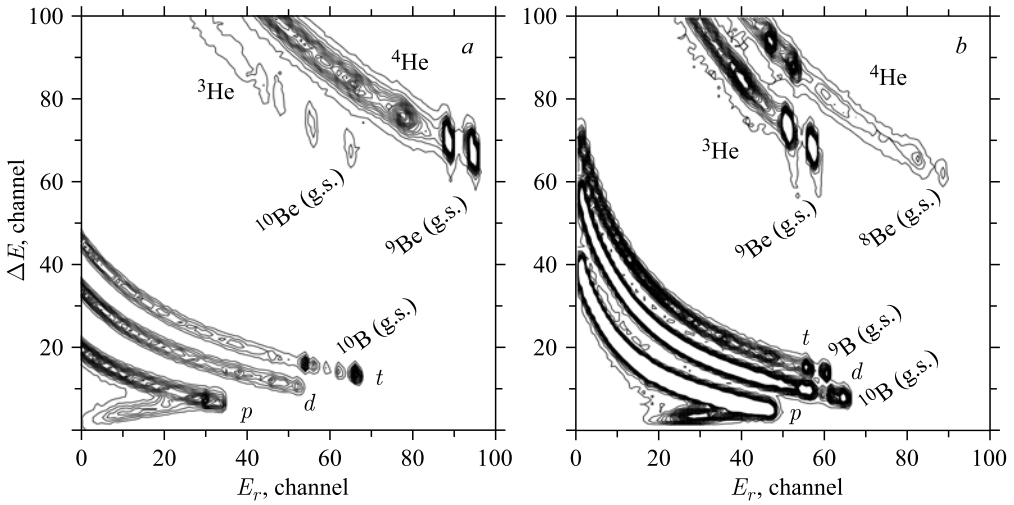

Fig. 1. $^4\mathrm{He} + {}^9\mathrm{Be}$ (*a*) and $^3\mathrm{He} + {}^9\mathrm{Be}$ (*b*) reactions product yields versus energy loss ΔE and residual energy E_r measured by the Si–Si(Li) telescope. The loci for ^{3,4}He, p, d, and t are indicated

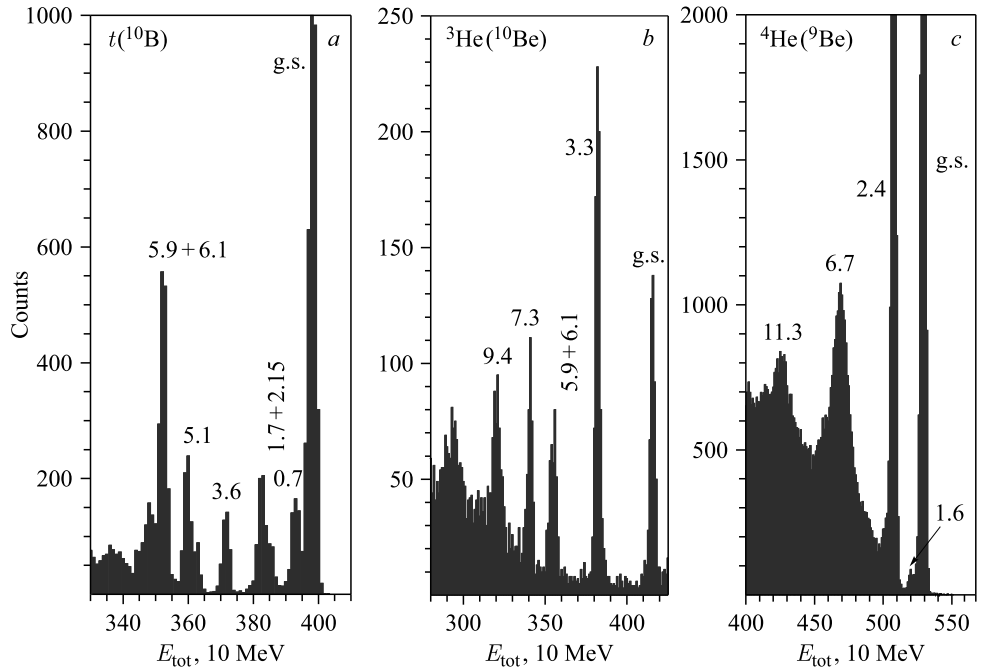

Fig. 2. Measured spectra of total energies for $^9\mathrm{Be}\,(\alpha, t)\,^{10}\mathrm{B}$ (*a*), $^9\mathrm{Be}\,(\alpha, {}^3\mathrm{He})\,^{10}\mathrm{Be}$ (*b*), and $^9\mathrm{Be}\,(\alpha, \alpha')\,^9\mathrm{Be}^*$ (*c*) reaction channels. The ground and most of the populated excited states of ^{10}B, ^{10}Be, and ^{9}Be are unambiguously identified

The overall energy resolution of the telescopes was nearly 200 keV. An example of two-dimensional plot (yield versus energy loss ΔE and residual energy E_r, measured by Si–Si(Li) detectors), is shown in Fig. 1, *a*. Excellent energy resolutions of both ΔE and E detectors allowed identifying ^{3,4}He, t, d, and p unambiguously.

The channel leading to the production of $^{7}\mathrm{Be} + {}^{6}\mathrm{He}$ has minimal probability due to the low Q-value. Other reaction channels take places at higher Q-values and consequently have larger cross sections, as is shown in Fig. 1. The production yield of ^{6}He starts to be visible only when plotting the z-axis (yield) in logarithmic scale; it is not shown in Fig. 1.

Comparing with the experimental technique of [6], we have the advantage to distinguish the particles p, d, t, ^{3}He, and ^{4}He and determine their total deposited energies. The total energies were obtained after energy calibration of all Si-detectors and summing of energy deposits in the ΔE and E_r detectors (see Fig. 2). All the observed peaks were identified and found to belong to the ground and excited states of ^{9}Be, ^{10}Be, and ^{10}B as the complementary products to detected particles ^{4}He, ^{3}He, and t, respectively.

We found an excellent agreement in the identification of the excited states observed in our experiment with those previously measured for ^{9}Be [5, 6], ^{10}Be [8, 9], and ^{10}B [8, 10]. Because the incident beam energy was rather high (about 15 MeV/u), the observed states are most likely populated in one-step direct transfer reactions.

1.2. ^{3,4}He (30, 40 MeV) + ^{9}Be Measurements. Next two runs of the experiment were performed at the K130 Cyclotron facility (Jyväskylä University) and later using the isochronous cyclotron U-120M of the Nuclear Physics Institute (NPI, Řež, Czech Republic). The beam energy of ^{4}He ions was 39 MeV (Řež) and 30 and 40 MeV in the case of ^{3}He ion beams (Řež and Jyväskylä, respectively). The experiments were performed at sufficiently high energy to ensure suppression of compound-nucleus contributions. The average beam current during the experiment was maintained at 10 nA. The self-supporting enriched (99%) Be target with 12 μm thickness was used.

The experimental conditions, detector system, and particle identification method were the same or similar to those realized in the first run. The $\Delta E - E$ distribution for the experiment performed with the ^{3}He beams is shown in Fig. 1, *b*. This plot demonstrates that the energy spectra of the detected ejectiles are the fingerprint of the complementary nuclei, which are the object of our interest.

2. RESULTS

2.1. Elastic and Inelastic Scattering. Measured angular distributions of differential cross sections of the ground and low-lying excited states for ^{9}Be are presented in Fig. 3. Due to low statistics we were not able to get the angular distribution for the first-excited $1/2^{+}$ state of ^{9}Be at 1.6 MeV.

Comparison with the results for the ground state of the previous measurements [6] (open symbols) demonstrates a good agreement at small scattering angles. The disagreement is observed at angles larger than 70° where our data are smaller than those of [6]. From the technical point of view, this difference could be explained by the absence of particle identification in [6], where Si(Li) detectors were used to measure the total energy only, without a ΔE measurement that would allow Z and A identification of the detected particles. Another reason could also be due to a different method used for subtraction of the continuum

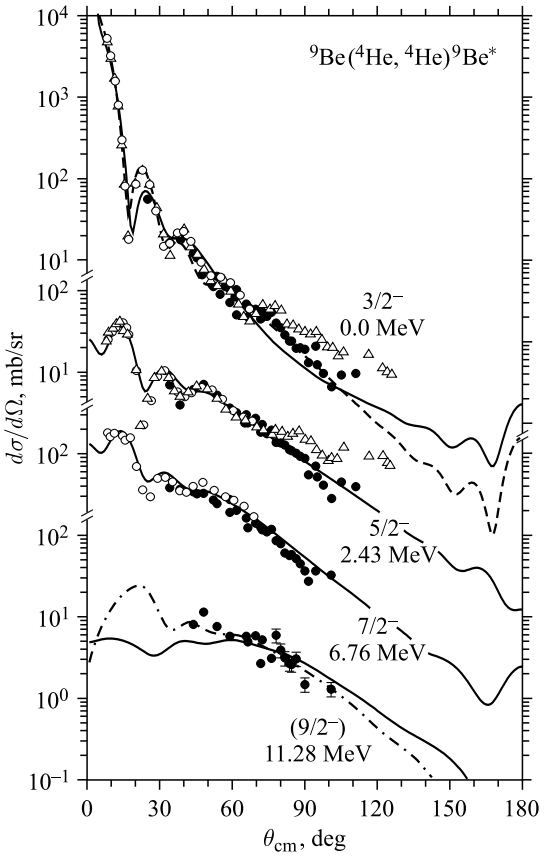

Fig. 3. Angular distributions of the differential cross sections for the ^{4}He (63 MeV) + ^{9}Be elastic and inelastic scattering. Data obtained in the present work are shown by solid symbols, data from [4, 5] are denoted by open symbols. Elastic scattering cross section was considered within optical model and shown by the dashed curve. Theoretical analysis (solid and dash-dotted curves) was performed within the coupled-channel approach assuming the rotational character of the excitations. Details of the calculation see in the text

under the peak. The same reasons are responsible for the difference between our data and those of [6] for the level at 6.76 MeV in the angular range 30–60° (see Fig. 3).

Figure 3 shows measured differential cross sections for the elastic and inelastic scattering (symbols) together with the results of theoretical calculations (curves) performed within the optical model and coupled-channel approach. Theoretical curves were obtained with the aid of NRV server optical model code [11] and the ECIS06 coupled-channel code [12, 13].

Firstly, let us consider the analysis of the elastic scattering cross section. The optical potential was chosen in the usual Woods–Saxon form

$$V(r) = -V_0 f(r, R_v, a_v) - iW_0 f(r, R_w, a_w),$$

where the function $f(r, R, a) = (1 + \mathrm{e}^{(r-R)/a})^{-1}$ and radii $R_i = r_i A^{1/3}$ depend on the mass of the heavier fragment A and corresponding reduced radius r_i. Potential parameters fitted within the optical model to the measured experimental data are listed in Table 1. Corresponding curve is shown in Fig. 3 as a dashed line and demonstrates a good agreement with obtained data. Note that the optical potentials recommended in the previous studies [5,6] do not provide a proper description of the elastic scattering data, since they were obtained by fitting the data in narrower angular range. Thus, in subsequent calculations in order to

Table 1. **Potential parameters used within the optical model and CC approaches**

System	V_0, MeV	r_v, fm	a_v, fm	W_0, MeV	r_w, fm	a_w, fm	r_C, fm
$\alpha + {}^{9}$Be	101.0	1.40	0.75	32.70	1.50	0.75	1.3
$\alpha + {}^{9}$Be (CC)	96.8	1.19	0.75	11.84	1.61	0.75	1.3
^{3}He $+ {}^{10}$Be [1]	95.0	0.95	0.82	8.00	1.60	0.73	1.1
$t + {}^{10}$B [2]	95.0	1.04	0.82	3.00	1.87	0.47	1.1
^{3}He $+ {}^{9}$Be	106.2	1.08	0.88	20.63	1.78	0.89	1.3
^{6}Li $+ {}^{6}$Li	81.9	1.08	0.96	11.72	2.38	0.89	1.2

[1] Parameters were taken from [14]. Real and imaginary depths and radii were modified within 10–15% of magnitude in order to fit experimental data on transfer to the ^{10}Be ground state.

[2] The ^{3}He $+ {}^{10}$Be parameters (taken from [14]) were used as initial set and then were fitted to reproduce experimental data on transfer to the ^{10}B ground state.

describe the entrance channel wave function we used the optical potential with the parameters listed in Table 1.

The simplest view of the ^{9}Be nucleus is that it is the Borromean system, i.e., strongly deformed three-body system consisting of two α particles held together by a weakly bound neutron. It is natural that different molecule-like states may appear in the excited states. The aim of the present experiment was to study the peculiarity of the angular distributions of elastic and inelastic scattering, mainly for $5/2^-$, $7/2^-$, and $9/2^-$ states, trying to learn more about their cluster structure.

Analysis of inelastic scattering data within the DWBA or CC approach allows one to extract the information on the deformation of an excited nucleus treating these states as collective rotational excitations. Corresponding coupling matrix elements, in addition to the radial form factor, include the deformation length $\beta_\lambda R_V$, where quantity β_λ is a deformation parameter, λ is a multipolarity of the transition defined by the transferred angular momentum, and $R_V = r_V A^{1/3}$ is an interaction radius depending on the mass A of the excited nucleus.

It is known [15–17] that ^{9}Be has a rotational band ($K^\pi = 3/2^-$) built on its ground state. In the previous studies only ground ($3/2^-$) and ($5/2^-$) excited states of the band were analyzed together in the CC framework. One may expect [18, 19] that all the angular distributions shown in Fig. 3 are related to the same rotational band. Note that the values of spin and parity of the 11.28 MeV state are uncertain. This level was listed either $7/2^-$ or $9/2^-$ state in the literature and databases. Following [16], we consider this state to belong to the rotational band and therefore to have spin-parity $9/2^-$.

The solid lines in Fig. 3 represent the results of the CC calculation within the symmetric rotational model taking also into account Coulomb excitation and reorientation terms. The ECIS06 code was employed. The parameters of the optical potential used in the CC calculations are given in Table 1 (marked as CC). They were fitted to the data shown in Fig. 3, using the optical model parameters as an initial set. It was found that inelastic scattering data for the first three states of the rotational band may be described well if one assumes $\beta_\lambda R_V = 1.574$ fm and $\beta_2 = 0.64$.

Quadrupole moment Q_{20} of the ^{9}Be nucleus is known to be $+53$ mb [20,21] indicating a prolate deformation for the ground state. The previous studies (e.g., [5,6]) have shown quite a large deformation parameter β_2 lying in the range from 0.5 to 0.7. It provided rather good agreement with our data on elastic and inelastic (2.43 and 6.76 MeV states) scattering. The obtained large β_2 value may be considered as the confirmation of the cluster structure of the low-lying states of ^{9}Be. However, it does not allow us to give unambiguous preference to the one of the possible configurations, for example, $\alpha + \alpha + n$ or $\alpha + {}^5$He.

In Fig. 3, one may see quite a poor agreement between the CC calculation and the experimental data (see the solid line in the bottom part of Fig. 3) in the case of 11.28 MeV state attributed as $9/2^-$ rotational state. It either may testify the fallacy of the assumption on the $9/2^-$ state nature or may indicate the different structure of this state. In order to improve the fits for this state, an additional hexadecapole term β_4 in the definition of the ^{9}Be radius was added. The dash-dotted line in Fig. 3 demonstrates the result obtained with the same β_2 value and $\beta_4 = 0.27$. It agrees much better with the data. There is an insignificant influence of the β_4 parameter on the cross sections for the $3/2^-$, $5/2^-$, and $7/2^-$ states. This may be the evidence of the different structure of the $9/2^-$ state of the ^{9}Be nucleus. It should be noted that data on inelastic scattering to the 11.28 MeV state were measured in the middle range of the angles, where two theoretical predictions are quite close. Thus, in order to draw final conclusion, additional measurements are required in a broader region of the scattering angles.

2.2. ^{9}Be (^{4}He, ^{3}He) ^{10}Be Reactions. If ^{9}Be shows molecular cluster structure [4], then ^{10}Be might be expected to show a more sophisticated internal structure. Molecular structure of the ^{10}Be nucleus is formed by two alpha particles and two neutrons. Such constitution attracts even more interest, since one neutron added to ^{9}Be makes the ^{10}Be nucleus as more compact configuration [15].

In this work, we performed measurements of the angular distributions for the ^{9}Be (^{4}He, ^{3}He) ^{10}Be reaction, leading to different ^{10}Be excited states. Angular distributions of the differential cross sections for the ground and low-lying excited states for ^{10}Be are plotted in Fig. 4, *a*. Results of the present experiment are shown by solid symbols; data from [6] are presented by the open symbols. Solid lines are the result of the finite-range DWBA calculations with the help of the DWUCK5 code [22] available via the Internet on the site of the NRV project [23].

In order to perform the DWBA calculations, the potential parameters listed in Table 1 were chosen to calculate distorted waves in the entrance and exit channels. The potential parameters for the exit channel $^3\mathrm{He} + {}^{10}$Be were chosen close to the potential recommended in [14]. The Q-value for the ^{9}Be (^{4}He, ^{3}He) ^{10}Be reaction channel is -13.8 MeV, that reduces the relative energy in the exit channel significantly. It legitimizes a slight variation of the optical model parameters for the exit channel (within 10%) for a better agreement of the calculations with the data. In the analysis reported below we varied only the depths of the real and imaginary parts within indicated limits.

The single-particle wave functions in the entrance and exit channels were defined within a standard potential model [24, 25]. The interaction for $n + {}^3$He system was chosen of the Gaussian form

$$V(r) = -V_G \exp\left(-\frac{r^2}{R_G^2}\right),$$

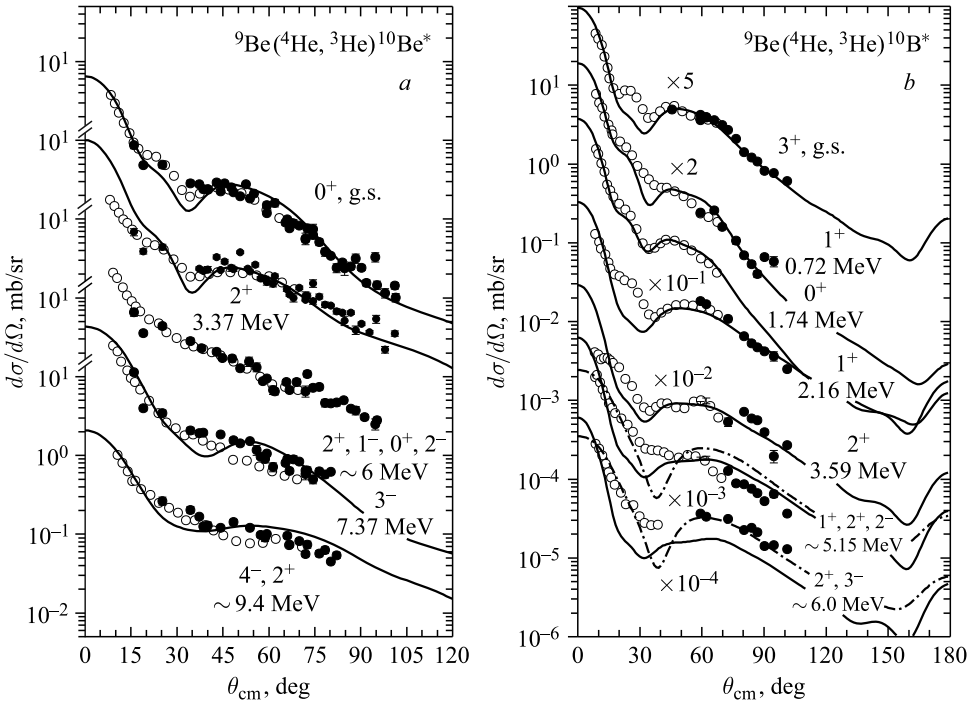

Fig. 4. Angular distributions of the differential cross sections for the ground and low-lying excited states of the ^{10}Be (*a*) and ^{10}B (*b*) nuclei formed in the ^{4}He + ^{9}Be reaction. Results of the present experiment are shown by solid symbols. Data from [5] are shown by open symbols. The curves demonstrate the calculation results explained in the text

where the radius $R_G = 2.452$ fm [25], while the potential depth V_G is fitted to reproduce the correct value of neutron binding energy $E_n = -20.58$ MeV in the ^{4}He nucleus. The $n + {}^{9}$Be potential in the final state was defined as a real Woods–Saxon potential with radius $R_V = 1.26\, A_{\rm Be}^{1/3}$ fm and diffuseness $a_V = 0.6$ fm. Potential depth V_0 was defined in the same manner as V_G parameter. For states unbound to the neutron emission in ^{10}Be, the neutron was assumed to be bound by 0.1 MeV, as is usually recommended [5].

Relative angular momentum of neutron state in the projectile or target-like fragment was fixed by the total momentum J and parity π conservation laws. In particular, the ground state of the $^{10}\mathrm{Be}\,(0^+) = n(1/2^+) + {}^{9}\mathrm{Be}\,(3/2^-)$ nucleus was considered as $1p_{3/2}$ neutron state, while the excited states of ^{10}Be with negative parity were treated as $1d_{5/2}$ neutron states. All spectroscopic properties of the ^{10}Be excited states are listed in Table 2.

The DWBA differential cross section for the considered stripping reactions can be compared with experimental data in the following way [22]:

$$\frac{d\sigma_{\rm exp}}{d\Omega} = S_f \frac{(2J_f+1)}{(2J_i+1)} \sigma_{\rm DW}(q),$$

where $J_i = 3/2$ and J_f are the angular momenta of the ^{9}Be target and the final state populated in ^{10}Be, respectively; $\sigma_{\rm DW}(\theta)$ is the output from DWUCK5; S_f are the target-like

Table 2. **Spectroscopic information for the ^{9}Be (^{4}He, ^{3}He) ^{10}Be and ^{9}Be (^{4}He, t) ^{10}B reactions as obtained from the DWBA analysis**

E_x, MeV	$J\pi$	l	S_f, [5]	S_f, present
^{9}Be $(\alpha, ^{3}$He$)$ ^{10}Be				
g.s.	0^+	1	1.58	1.65
3.368	2^+	1	0.38	1.00
5.958	2^+	1	$\leqslant 0.73$	$\leqslant 1.40$
5.960	1^-	2	$\leqslant 0.14$	$\leqslant 0.43$
6.179	0^+	1	—	—
6.263	2^-	2	0.08	$\leqslant 0.26$
7.371	3^-	2	0.26	0.28
7.542	2^+	1	—	—
9.27	4^-	2	$\leqslant 0.18$	0.10
9.56	2^+	1	—	0.23
^{9}Be (α, t) ^{10}B				
g.s.	3^+	1	0.89	0.59
0.781	1^+	1	1	1.0
1.76	0^+	1	1.58	1.38
2.1	1^+	1	0.52	0.30
3.6	2^+	1	0.28	0.23
5.11	2^-	2	$\leqslant 0.27$	$\leqslant 0.16$
5.16	2^+	1	$\leqslant 1.85$	$\leqslant 0.75$
5.18	1^+	1	$\leqslant 3.14$	$\leqslant 1.0$
5.93	2^+	1	0.48	$\leqslant 0.95$
6.13	3^-	2	0.24	$\leqslant 0.19$

fragment spectroscopic factors. Figure 4 demonstrates how good the obtained absolute values of the spectroscopic factors S_f are, which were obtained from the comparison of the measured angular distributions and DWUCK5 calculations for the different ^{10}Be final states. The values of the spectroscopic factors are listed in Table 2 together with S_f reported in [5].

It is seen that the obtained cross sections agree well with the data. The spectroscopic factors extracted from our analysis are very close to the ones listed in [5] (see Table 2), except for the ^{10}Be state at 3.368 MeV, where spectroscopic values differ by more than a factor of two. The reason for this discrepancy is the following. The spectroscopic factor in our work was defined by adjusting the theoretical curve to the data measured in the middle angle domain, while in [5] it was fitted to the forward experimental points near $\theta_{\rm cm} \approx 10^\circ$.

In spite of the high energy resolution, we were not able to separate the excited states nearby 6 MeV. Low statistics did not allow us to observe the 2^+ state at 7.54 MeV. The experimental cross sections corresponding to two overlapping states near 9.5 MeV were described as a sum of DWUCK5 outputs multiplied by the corresponding spectroscopic factors. Table 2 contains the S_f values providing the best fit.

Note that in order to describe the data one needs much smaller radius of the real part of the optical potential for the exit channel ($r_V = 0.95$ fm) in comparison to the radius in the entrance channel ($r_V = 1.40$ fm) that indicates the compactness of the ^{10}Be nucleus.

Nuclear charge radii of ^{7,9,10}Be have been measured by high-precision laser spectroscopy [18, 19]: the charge radius decreases form ^{7}Be to ^{10}Be. Comparing the Coulomb

parameter r_C with that of ^{9}Be, we obtained a smaller value of r_C for ^{10}Be. In [18, 19], the decrease was explained as probably caused by the clusterization of ^{7}Be into an α and triton clusters, whereas ^{9,10}Be were considered to be $\alpha + \alpha + n$ and $\alpha + \alpha + n + n$ systems, respectively, and were more compact. The experimental trend was shown [15] to change beyond ^{10}Be with an increase of the charge radius with atomic mass. Furthermore, the large experimental value of the charge radius for ^{12}Be is consistent with a breakdown of the $N = 8$ shell closure.

2.3. ^{9}Be (^{4}He, t) ^{10}B Reactions. Differential cross sections versus angles in cm-system for the ground and low-lying excited states of ^{10}B are plotted in Fig. 4, *b*. Results of the present experiment are shown by solid symbols, and data from [5] are presented as open symbols. DWBA calculations [23] for the ^{9}Be (α, t) ^{10}B reaction were performed with the DWUCK5 code [22] fitting the differential cross sections for the ground and low-lying states. Results are shown by the solid lines in Fig. 4. One may notice a very good agreement between data obtained in [5] and our measurements. Theoretical results (solid and dash-dotted curves) fairly reproduce the data in case of well-defined final states. For the unresolved mixture of states at excitation energies of about 5.15 and 6 MeV, one may conclude that negative parity states corresponding to $l = 2$ (shown by dash-dotted curves) provide a better agreement with the data than positive parity ones ($l = 1$, solid curves).

Spectroscopic factors S_f for the different states populated in the reaction ^{9}Be $(^4$He, $t)$ ^{10}B are listed on the right side of Table 2. For the data corresponding to the mixture of a few levels an upper limit of spectroscopic factor was obtained, describing the data by one component only. S_f values are in a good agreement with those reported in the literature.

2.4. Multiplet $A = 10$. The structure of ^{10}Be, ^{10}B, and ^{10}C nuclei was usually considered as two α-clusters in the presence of two extra nucleons. Level diagrams for the low-energy excited states for these nuclei are shown in the right panel of Fig. 5. One may see that

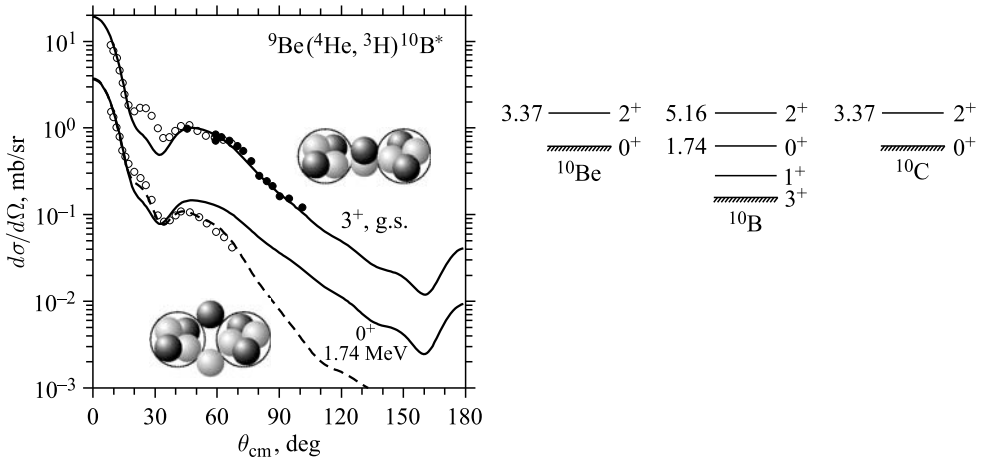

Fig. 5. On the left side the differential cross sections for ^{9}Be $(^4$He, $t)$ ^{10}B reaction leading to the ground and 1.74 MeV excited states of ^{10}B nucleus are presented. Solid symbols show the results of the present experiment, open ones are the data from [5]. Curves show the results of DWBA calculations (see the text for details). On the right side the level diagrams of low-lying states of members of the $A = 10$ isobaric multiplet are shown

the ^{10}B ground state is shifted down by 2 MeV approximately. It may be treated as a three-cluster configuration $^{10}\mathrm{B} = \alpha + d + \alpha$, where the pairing of proton and neutron results in formation of a deuteron cluster inside. The 3^+ spin of this state also supports this assumption. The 1.74 MeV excited state might be considered as a state where the deuteron cluster becomes unbound. Thus, the four-cluster configuration $^{10}\mathrm{B}\,(0^+,\ 1.74\ \mathrm{MeV}) = \alpha + p + n + \alpha$ with uncorrelated proton and neutron manifests itself. Two mirror ground states in ^{10}Be and ^{10}C in this case have to be of similar structure $\alpha + N + N + \alpha$. One of the consequences of such an internal organization is the absence of the di-neutron component in the ^{10}Be ground state wave function.

Difference in the structure of the ground state and the 1.74 MeV state in ^{10}B may also reveal itself in the difference of optical potentials for these exit channels. In Fig. 5, the corresponding experimental data are compared with the results of DWBA calculations performed in the same manner as for the $^3\mathrm{He} + {}^{10}\mathrm{Be}$ exit channel. Solid curves show theoretical cross sections obtained with the exit channel optical potential from Table 1. This potential was chosen on the basis of OM potential compilation from [14] with additional adjustment of parameters to the present data, since [14] contains the recommended optical potential for the lower collision energies. One may see quite a good agreement between the calculation and data on the case of proton transfer, leading to the ^{10}B ground state. Applying the same potential for the transfer to the 1.74 MeV state, one gets the noticeable overestimation in the cross section at large angles. We found that in order to improve the agreement in the last case it is necessary to use the following parameters: $V_0 = 85$ MeV, $r_V = 1.14$ fm, and $W_0 = 8$ MeV. Corresponding result is shown in Fig. 5 by the dashed curve and demonstrates an excellent fit of the data. The obtained parameters turn out to be close to the OM potential for $^3\mathrm{He} + {}^{10}\mathrm{Be}\,(\mathrm{g.s.})$ channel.

2.5. Multinucleon Transfer in ^{3}He + ^{9}Be Reaction. Here we report the data on the $^3\mathrm{He} + {}^9\mathrm{Be}$ interactions followed with the triton and ^{3}He pickup at the incident energy of

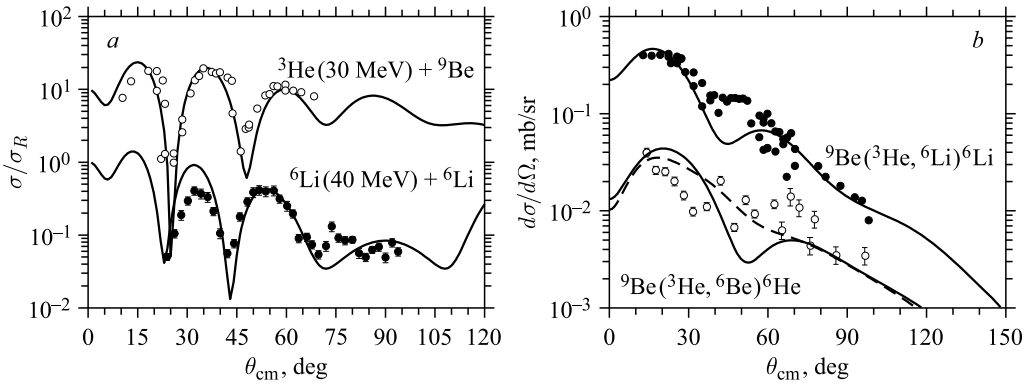

Fig. 6. *a*) The elastic scattering angular distribution for the $^3\mathrm{He} + {}^9\mathrm{Be}$ and $^6\mathrm{Li} + {}^6\mathrm{Li}$ reactions. The curves correspond to the optical model fit with parameters from Table 1. *b*) Differential cross section for the ^{3}H and ^{3}He pickup channels of the $^3\mathrm{He} + {}^9\mathrm{Be}$ reaction at the energy of 40 MeV. Curves show the calculations within DWBA (see the text for details). Experimental data are from this work except the $^6\mathrm{Li} + {}^6\mathrm{Li}$ data which are from [26]

40 MeV. These reaction channels are of specific interest since they provide the direct information on the cluster structure of initial and final states.

First of all, we fit the optical model parameters in order to describe the elastic scattering data. The data for the entrance channel were measured during the reported experiment, while the data for the $^{6}\mathrm{Li} + {}^{6}\mathrm{Li}$ elastic scattering were found in [26]. Obtained potential parameters are listed in Table 1. In Fig. 6, *a*, the elastic scattering cross sections are shown. One may see the acceptable agreement between the data and optical model calculations. It is necessary to note one peculiarity of the $^{6}\mathrm{Li} + {}^{6}\mathrm{Li}$ optical potential which has a very expanded imaginary part. Indeed, the radius R_w for this combination is more than 4 fm, while the real part has radius less than 2 fm. The optical potentials fitting the data at different energies [26] demonstrate the same properties. There is no clear explanation of this fact.

In order to perform the DWBA calculation of the transfer reactions, one defined the bound state parameters in the entrance and exit channels. The $^{9}\mathrm{Be}\,(3/2^{-})$ ground state is treated now as a two-body system $^{3}\mathrm{H}\,(1/2^{+}) + {}^{6}\mathrm{Li}\,(1^{+})$ with binding energy $\varepsilon_b = -17.7$ MeV. According to the selection rules on the momentum coupling and the parity conservation, we can define the relative state as $2p_{3/2}$ one. The Woods–Saxon potential with parameters $V_0 = -142.6$ MeV, $r_v = 1.05$ fm, $a_v = 0.5$ fm was applied to describe the $^{3}\mathrm{H} + {}^{6}\mathrm{Li}$ bound state. In the same manner, the bound state $^{6}\mathrm{Li} = {}^{3}\mathrm{H} + {}^{3}\mathrm{He}$ in the exit channel is treated. The Gaussian potential with depth $V_0 = -148.6$ MeV and radius $r_v = 1.25$ fm describes the $2s_{1/2}$ state with binding energy $\varepsilon_b = -15.8$ MeV.

In Fig. 6, *b*, the solid dots and corresponding curve show the experimental data and DWBA calculation of the angular distribution for the triton pickup reaction. The figure demonstrates a fairly good agreement between the data and calculations with spectroscopic factors $S_i S_f = 0.9$, confirming the large contribution of the $(^{3}\mathrm{H} + X)$ configuration into the ground state wave functions of the $^{9}\mathrm{Be}$ and $^{6}\mathrm{Li}$ nuclei.

Following the same procedure, we calculated the $^{3}\mathrm{He}$ pickup reaction. The bound state parameters for both channels were chosen the same except the binding energies and depth of the potentials. The energy of the $^{3}\mathrm{He} + {}^{6}\mathrm{He}$ system is -21.2 MeV, that results in the potential depth $V_0 = -151.4$ MeV. The separation energy of the $^{3}\mathrm{He}$ from the $^{6}\mathrm{Be}$ nucleus is 11.5 MeV. The solid curve together with open symbol in Fig. 6, *b* demonstrates the differential cross section calculated using the same distortion potentials. The obtained spectroscopic factor for this reaction is 0.6.

One may see from Fig. 6 that in spite of comparable spectroscopic factors the cross sections for the considered reactions are approximately one order of magnitude different. The reason is mainly the Q-values which are -1.9 MeV for the $^{3}\mathrm{H}$ pickup and -9.7 MeV in the case of $^{3}\mathrm{He}$ transfer.

One may see that the data for the $^{6}\mathrm{He} + {}^{6}\mathrm{Be}$ exit channels are in a poor agreement with the calculations. Since both nuclei in this exit channel are exotic, weakly bound, and even unstable, it is appropriate to analyze the dependence of the cross section on the model parameters. Since the $^{6}\mathrm{Be}$ nucleus is unstable to the double-proton emission, one may expect, in particular, the extended spatial distribution for this nucleus. To simulate it, we increase the potential radius for the bound state in the exit channel to the value $r_v = 1.9$ fm (more than 50%), that leads to the depth $V_0 = -79.8$ MeV. Resulting cross section is shown by the dashed curve in Fig. 6. It is very promising to see that the difference in the calculated cross sections are mainly at small scattering angles where the data are measured. It stimulates further investigation of the reactions of such kind with better statistics.

CONCLUSIONS

Angular distributions of the differential cross sections for the ^{9}Be (α, α) ^{9}Be*, ^{9}Be $(^{4}$He, ^{3}He$)$ ^{10}Be, and ^{9}Be $(^{4}$He, $t)$ ^{10}B reactions were measured. Experimental angular distributions were described within the optical model, coupled channel approach, and distorted-wave Born approximation. Spectroscopic factors for the ground and excited states of ^{10}B and ^{10}Be were deduced. We found a pretty good agreement between our results and the previous data.

The performed analysis of the experimental data shows that the potential parameters are quite sensitive to the exit channel and hence to the cluster structures of the excited states. It allows one to make the general conclusions and assumptions on the peculiarities of the internal structure of the tested nuclei. To study their cluster structure, a complicated experiment is planned in which decay of excited states by cluster emission will be investigated. However, to distinguish break-up into ^{4}He and ^{5}He will not be a trivial kinematical problem.

The values $9/2^{-}$ were assigned to the spin and parity of the 11.28 MeV state in ^{9}Be. The obtained large β_2 deformation confirms the cluster structure of the low-lying states of ^{9}Be. However, it does not allow us to give an unambiguous preference to one of the possible configurations $\alpha + \alpha + n$ or $\alpha + {}^{5}$He. In order to improve the agreement between the theoretical prediction and the experimental data, related to the $^{9}/2-$ state, an additional hexadecapole term β_4 is suggested in the definition of the ^{9}Be radius.

Our analysis supports an evidence of the compactness of the ^{10}Be ground state. It was found that in order to describe the data one needs a much smaller radius of the real part of the optical potential for the exit channel ($r_V = 0.95$ fm) in comparison to the radius in the entrance channel ($r_V = 1.40$ fm).

The comparison of the angular distributions of the differential cross sections for the isobaric analog states of ^{10}Be and ^{10}B was done. The structure of ^{10}Be, ^{10}B, and ^{10}C nuclei was usually considered as two α-clusters in the presence of two extra nucleons. It is shown that the ^{10}B ground state could be treated as a three-cluster configuration $^{10}\mathrm{B} = \alpha + d + \alpha$, where the pairing of proton and neutron results in formation of a deuteron cluster inside ^{10}B. In the case of the 1.74 MeV excited state, the deuteron cluster becomes unbound and the system is considred as the four-body configuration, where two α-clusters coexist with an uncorrelated proton and neutron pair.

The cross section of the ^{3}H and ^{3}He transfer was measured in the $^{3}\mathrm{He} + {}^{9}$Be collision at energy of 40 MeV. Proposed optical potential provides a good fit of the elastic scattering in the entrance and exit channels. The DWBA calculations are well agreed with the transfer reaction data. The spectroscopic factors of both reactions are close to unit that confirms a significant contribution of the considered cluster configurations. We show also the possibility to extract the structural information from the comparative analysis of the ^{9}Be $(^{3}$He, ^{6}Li$)$ ^{6}Li and ^{9}Be $(^{3}$He, ^{6}Be$)$ ^{6}He reactions.

Acknowledgements. We would like to thank the JYFL Accelerator Laboratory and NPI (Řež) for giving us the opportunity to perform this study and the cyclotron staff for the excellent beam quality. This work was supported in part by the Russian Foundation for Basic Research (project Nos. 13-02-00533 and 14-02-91053), the CANAM (IPN ASCR), by grants to JINR (Dubna) of the Czech and Polish Republics, and by mobility grant from the Academy of Finland.

REFERENCES

1. *Bertulani C. A., Canto L., Hussein M. S.* The Structure and Reactions of Neutron-Rich Nuclei // Phys. Rep. 1993. V. 226. P. 281.
2. *Jonson B.* Light Dripline Nuclei // Phys. Rep. 2004. V. 389. P. 1.
3. *Penionzhkevich Yu. E.* Super Neutron-Rich Nuclei: Results of Prospects of Investigations // Phys. At. Nucl. 2014. V. 77. P. 75; Yad. Fiz. 2014. V. 77. P. 79.
4. *von Oertzen W.* // Proc. of Intern. Symp. on Exotic Nuclei, 2009 / Eds. Yu. Penionzhkevich and S. Lukyanov. New York: AIP, 2009.
5. *Harakeh M. et al.* Strong Coupled-Channels Effects in the $^{9}\mathrm{Be}\,(\alpha, t)\,^{10}\mathrm{B}$ Reaction // Nucl. Phys. A. 1980. V. 344. P. 15.
6. *Roy S. et al.* Coupled Channel Folding Model Description of α Scattering from ^{9}Be // Phys. Rev. C. 1995. V. 52. P. 1524.
7. *Lukyanov S. M. et al.* // J. Phys. G: Nucl. Part. Phys. 2014. V. 41, No. 3. P. 035102.
8. *Tilley D. et al.* Energy Levels of Light Nuclei // Nucl. Phys. A. 2004. V. 745. P. 155.
9. *Bohlen H. G. et al.* Structure of ^{10}Be from the $^{12}\mathrm{C}\,(^{12}\mathrm{C},\,^{14}\mathrm{O})\,^{10}\mathrm{Be}$ Reaction // Phys. Rev. C. 2007. V. 75. P. 054604.
10. *Miura K. et al.* The $^{9}\mathrm{Be}\,(d, n)\,^{10}\mathrm{B}$ Reaction at 25 MeV // Nucl. Phys. A. 1992. V. 539. P. 441.
11. *Zagrebaev V., Denikin A., Alekseev A.* Optical Model of Elastic Scattering. http://nrv.jinr.ru/nrv/. 2000. Nuclear Reaction Video Project.
12. *Raynal J.* Computing as a Language of Physics // Proc. of ICTP Intern. Seminar Course, Trieste, Italy, 1971. Vienna: IAEA, 1972.
13. *Raynal J.* Computer Code ECIS06. Unpublished. 2006.
14. *Perey C., Perey F.* Compilation of Phenomenological Optical-Model Parameters 1969–1972 // At. Data Nucl. Data Tables. 1974. V. 13. P. 293.
15. *Koike Y.* ^{9}Be: A Gateway Nucleus into Heavier Nuclei? arXiv:nucl-th/0201075. 2008.
16. *Ajzenberg-Selove F.* Energy Levels of Light Nuclei $A = 5{-}10$ // Nucl. Phys. A. 1988. V. 490. P. 1.
17. *Votava H. et al.* Proton Scattering from ^{9}Be between 6 and 30 MeV and the Structure of ^{9}Be // Nucl. Phys. A. 1973. V. 204. P. 529.
18. *Nörtershäuser W. et al.* Nuclear Charge Radii of ^{7,9,10}Be and the One-Neutron Halo Nucleus ^{11}Be // Phys. Rev. Lett. 2009. V. 102. P. 062503.
19. *Krieger A. et al.* Nuclear Charge Radius of ^{12}Be // Phys. Rev. Lett. 2012. V. 108. P. 142501.
20. *Blachman A. G., Lurio A.* Hyperfine Structure of the Metastable $(1s^2 2s2p)\,^3p$ States of $_4\mathrm{Be}^9$ and the Nuclear Electric Quadrupole Moment // Phys. Rev. 1967. V. 153. P. 164.
21. *Stone N.* Table of Nuclear Magnetic Dipole and Electric Quadrupole Moments // At. Data Nucl. Data Tables. 2005. V. 90. P. 75.
22. *Kunz P.* Computer Code DWUCK5. http://spot.colorado.edu/ kunz/DWBA.html.
23. *Zagrebaev V., Denikin A., Alekseev A.* DWBA for Nucleon Transfer Reactions. http://nrv.jinr.ru/nrv/webnrv/transfer/. 2009. Nuclear Reaction Video Project.
24. *Dubovichenko S. B., Dzhazairov-Kakhmanov A. V.* Electromagnetic Effects in Light Nuclei within Cluster Potential Model // Phys. Part. Nucl. 1977. V. 28. P. 1529.
25. *Denikin A. S., Zagrebaev V. I., Descouvemont P.* Generalized Optical Potential for Weakly Bound Nuclei: Two-Cluster Projectiles // Phys. Rev. C. 2009. V. 79. P. 024605.
26. *Potthast K. et al.* Global Optical Model Potentials for Symmetrical Lithium Systems: $^{6}\mathrm{Li} + {}^{6}\mathrm{Li}$, $^{7}\mathrm{Li} + {}^{7}\mathrm{Li}$ at $E_{\mathrm{lab}} = 5{-}40$ MeV // Nucl. Phys. A. 1997. V. 614. P. 95.

Received on March 31, 2015.